



TECHNICAL ARTICLE

Role of Friction Time on the Joint Characteristics of Continuous Drive Friction-Welded Inconel 718 and EN24 Steel

V.T. Gaikwad, M.K. Mishra, V.D. Hiwarkar, and R.K.P. Singh

Submitted: 4 January 2022 / Revised: 14 June 2022 / Accepted: 29 June 2022 / Published online: 29 August 2022

In the present research work, dissimilar metal joints of nickel-based superalloy (IN718) and low-alloy steel (EN24) round bars were carried out by using continuous drive friction welding. The joining of specimens was performed by varying friction time in the range of 2-10 s and keeping other welding parameters (friction pressure, 50 bar; upset pressure, 80 bar; upset time, 3 s; and rotational speed, 1400 rpm) constant. The main focus is to understand the characteristics of weld interface (WI), burn-off length and mechanical behavior of weld samples. It is noteworthy that significant changes in the microstructure caused variation in hardness across the weld interface. Moreover, it was observed that burn-off length increased linearly from 4.2 to 12.9% with increasing friction time. The tensile test results revealed that joint efficiency ~ 100% can be achievable by selecting the appropriate parameters.

Keywords burn-off length, dissimilar friction welding, friction time, mechanical properties, microstructure

1. Introduction

Joints of dissimilar metal are used primarily due to cost saving and utilization of dual material properties for the manufacturing of engineering components (Ref 1). Moreover, the combination of different materials has greater significance in automotive, aerospace, petroleum, nuclear and mining industries (Ref 2). Inconel (IN718) is a family of nickel-based superalloys with excellent corrosion resistance and high mechanical strength at elevated temperatures. These exceptional mechanical properties of IN718 at high temperature can be derived from the presence of solid solution strengthening elements (Fe, Cr, Mo and Nb substitute in Ni matrix) and strengthening precipitates viz. γ' – $[\text{Ni}_3\text{AlTi}]$ and γ'' – $[\text{Ni}_3\text{Nb}]$ (Ref 3). On the other hand, EN24 is versatile steel widely used in industry for manufacturing of transmission components due to its excellent hardenability, formability, weldability and adequate mechanical properties (Ref 4). Joints of Inconel and steel are essential in some high-temperature critical applications such as turbochargers and aeroengines components (Ref 2-5).

V.T. Gaikwad, Kalyani Centre for Technology and Innovation, Bharat Forge Limited, Pune 411036, India; and Department of Materials Engineering, Defense Institute of Advance Technology, Pune 411025, India; M.K. Mishra, Department of Metallurgical and Materials Engineering, Malaviya National Institute of Technology Jaipur, Jaipur 302017, India; V.D. Hiwarkar, Department of Materials Engineering, Defense Institute of Advance Technology, Pune 411025, India; and R.K.P. Singh, Kalyani Centre for Technology and Innovation, Bharat Forge Limited, Pune 411036, India. Contact e-mail: prajwalvijay75@gmail.com.

However, joining of these materials is a challenging task to researchers.

Literature shows that welding of IN718 superalloy with conventional fusion welding method is problematic due to boron/niobium segregation, laves phase formation and liquation cracking (Ref 6). To overcome these issues, solid-state joining is a feasible solution. Among the solid-state welding processes, friction welding (FW) and friction stir welding (FSW) are well-known innovative joining methods (Ref 7). However, FSW is mostly suitable for joining of flat plates with rectangular or square shapes. By using FSW methods, joining of round-shape components such as for turbocharger application (IN718 and EN24) is difficult. In FW, joining can be accomplished at a temperature well below the melting point by producing mechanical friction heat. Since the welding is performed in solid state, it has many benefits like smaller heat-affected zone (HAZ), easy surface preparation, absences of filler metals and dispensable of inert atmosphere during welding (Ref 2, 5, 7).

Recently, several studies on FW of different materials have been reported by researchers (Ref 2, 5, 19, 21). Literature shows that FW can be effectively used for joining of similar and also dissimilar materials. V.T. Gaikwad et al. studied the microstructure and mechanical properties of EN24 and IN718 friction-welded samples. The joint was observed to be metallurgically sound with uneven flash formation due to difference in thermal conductivity and yield strength of two metals (Ref 8). H. C. Dey et al. produced a stronger weld of titanium and 304L stainless steel (fracture occurs in titanium during tensile test) by optimizing the welding parameters (Ref 9). Tiley et al. investigated the strengthening mechanisms associated with the as-welded microstructure developed during inertia friction welding of dissimilar superalloys LHSR and Mar-M247. They reported improvement in hardness in the vicinity of the weld interface due to the refined dispersion of γ' precipitates and γ grains (Ref 10). Damodaram et al. have also reported refinement of grains in weld interface of IN718 superalloy which is attributed to dynamic recrystallization (Ref 11).

In order to improve joint strength of IN718 superalloy, postweld heat treatment (PWHT) is suggested by Wang et al. (Ref 12). S. Vardhan Lalam et al. have investigated the effect of postweld heat treatment on FW joint of IN718 and EN24. They concluded that postweld heat treatment is beneficial for improving the joint strength but reducing the fracture toughness due to complex precipitates (Ni_3Al_4 , Fe_3Mn_7 and $\text{Al}_{0.9}\text{Ni}_{1.1}$) (Ref 13). Li et al. have investigated the effect of friction time on the mechanical properties of continuous drive friction-welded samples of (Ti6Al4V) titanium alloy and (SUS321) stainless steel. The results show that the tensile strength increases with friction time under experimental conditions. However, fracture occurred along the joint interface, due to formation of intermetallic compounds like FeTi , Fe_2Ti , $\text{Ni}_3(\text{Al}, \text{Ti})$ and $\text{Fe}_3\text{Ti}_3\text{O}$ and many other phases between the two base metals elements (Ref 14). For enhancement of mechanical properties and subsequently avoid the formation of brittle intermetallic phases at FW joints, D. Meshram et al. attempted to introduce silver interlayer (Ref 15). Ogura Tomo et al. have been reported that formation of intermetallic compound can be suppressed by adding Au-Ni interlayer for joining of Ti-6Al-4V and IN718 superalloys (Ref 16). From the literature, it appears that despite the development of various new technologies, achieving defect-free and metallurgically sound-welded joint seem to be challenging task for researchers.

According to authors knowledge, limited research work on dissimilar friction welding of IN718 and EN24 has been reported in the literature (Ref 8, 13). In our previous work (Ref 8), joining was performed by keeping friction time constant and the microstructures of three distinct weld zones—the weld interface (WI)/thermo-mechanically affected zone (TMAZ), the heat-affected zone (HAZ) and the base metal were examined. However, in this study attempts are made to understand the role of friction time on the weld joint characteristics and subsequent changes in mechanical properties. Furthermore, the relationship between friction time and burn-off length is also investigated.

2. Experimental Procedures

In this study, alloy of IN718 and EN24 was used for continuous drive friction welding. The samples were machined using lathe machine to get cylindrical shape having diameter— $\text{Ø}16$ mm and length—65 mm. Prior to welding, the interaction faces of the specimens were ground smoothly for easily flow of the flash and obtaining defect-free weld joints. The elemental compositions of the parent materials are listed in Table 1.

The welding was performed using continuous drive friction welding machine with capacity of 120 KN (Model FWT-12) at Friction Welding Technologies, Pune, India. The following welding parameter values were used: friction pressure (50 bar), upset pressure (80 bar), upset time (3 s) and rotational speed

(1400 rpm). The friction times for specimens 1, 2, 3, 4 and 5 were kept 2, 4, 6, 8 and 10 s, respectively. Experiments were performed by holding IN718 and EN24 specimen in rotating and stationary chuck, respectively, as shown in Fig. 1(a). The images of friction-welded samples are presented in Fig. 1(b).

After welding, specimens were extracted from axial cross section. These specimens were mounted and polished for microstructural analysis. In order to reveal the microstructure, Kallings reagent and 2% Nital were used for revealing the microstructure of alloy IN718 and EN24 side, respectively. For electron backscatter diffraction (EBSD) study, electro-polishing was performed using electrolyte containing 30% perchloric acid in ethanol. The microstructure investigations of welded samples were carried out by using optical microscope (OM) and scanning electron microscope (SEM) equipped with EBSD gun. The EBSD scans were performed at a step size of $0.4 \mu\text{m}$. The deformed, substructured and recrystallized fraction were analyzed using the channel 5 software provided by HKL Technology. Moreover, for identification of different phases, the samples were exposed to x-ray using copper K_α ($\lambda = 1.54056 \text{ \AA}$) radiation within 2θ range of $20\text{--}100^\circ$. Microhardness of welded specimens was measured across the weld interface using a Zeiss microhardness testing machine. Measurement was taken by applying 500 gf load for dwell times of 10 s. Joint strength of specimens was evaluated by tensile tests. Specimens for tensile testing were prepared as per ASTM-E8 standard keeping weld line at the center of the gauge length. The tests were conducted at room temperature with a cross head speed of 0.03 mm sec^{-1} .

3. Results and Discussion

3.1 Microstructure Analysis of Weld Joints

The image of friction-welded joint of IN718 and EN24 is shown in Fig. 2(a). It can be seen that flash width of IN718 is lower compared to flash width of EN24. As-received microstructure of IN718 and EN24 is given in Fig. 2(b), and (c), respectively. As-received IN718 rods were solution-treated and aged. The microstructure of the IN718 contained strengthening precipitates (γ' , γ''), MC-type carbides and needle-shaped delta phase (δ) in a γ (Ni) matrix (Fig. 2b) and (Fig. 8c, d). The detail descriptions of these phases are given in Sect. 4.1. The EN24 steel rods were in annealed condition. The microstructure consists of sphere-like carbides in a ferrite matrix (Fig. 2c).

Figure 3 shows the SEM and EBSD image quality maps of WI/TMAZ zones welded with 2 s, 6 s and 10 s friction times, respectively. It can be clearly observed that all joints are defect-free with approximate in straight line. Moreover, the SEM micrograph of WI/TMAZ of EN24 side shows martensite (plate morphology) microstructure (Fig. 3a-c) Therefore, it confirms that temperature of WI/TMAZ reached into austenitic region. Literature also shows that temperature in this zone reaches up

Table 1 Chemical composition (wt.%) of IN718 and EN24 alloys

Elements	Ni	Cr	Nb	Mo	Ti	Al	C	Mn	Si	Cu	Fe
Alloy IN718	53.60	17.82	5.05	3.01	0.66	0.45	0.08	0.04	16.91
Alloy EN24	1.53	1.29	...	0.25	0.41	0.61	0.26	...	Bal.

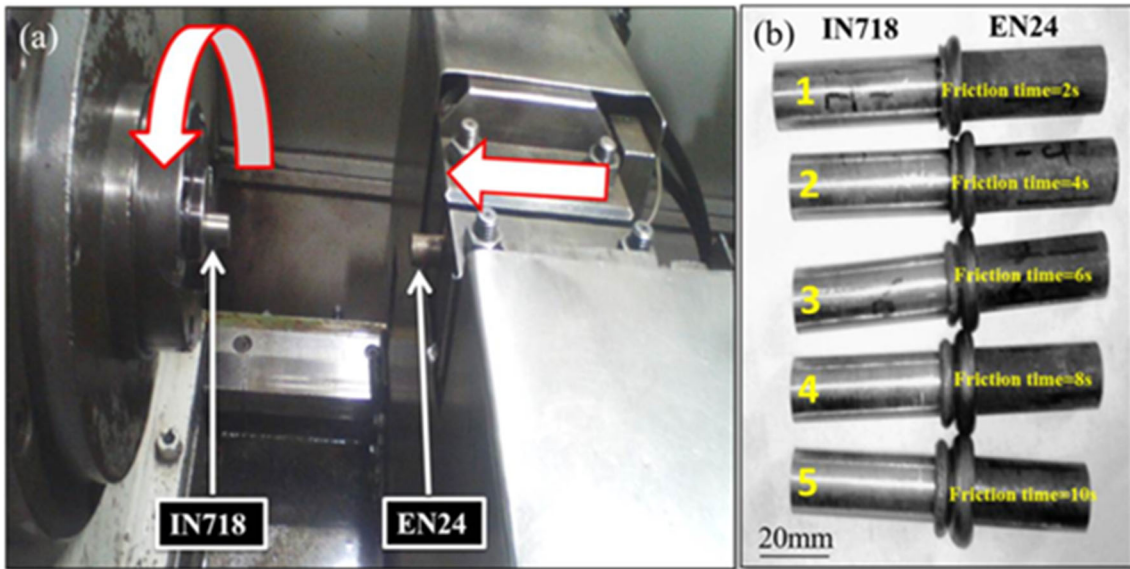


Fig. 1 (a) Friction welding setup, (b) images of FW samples for different friction time

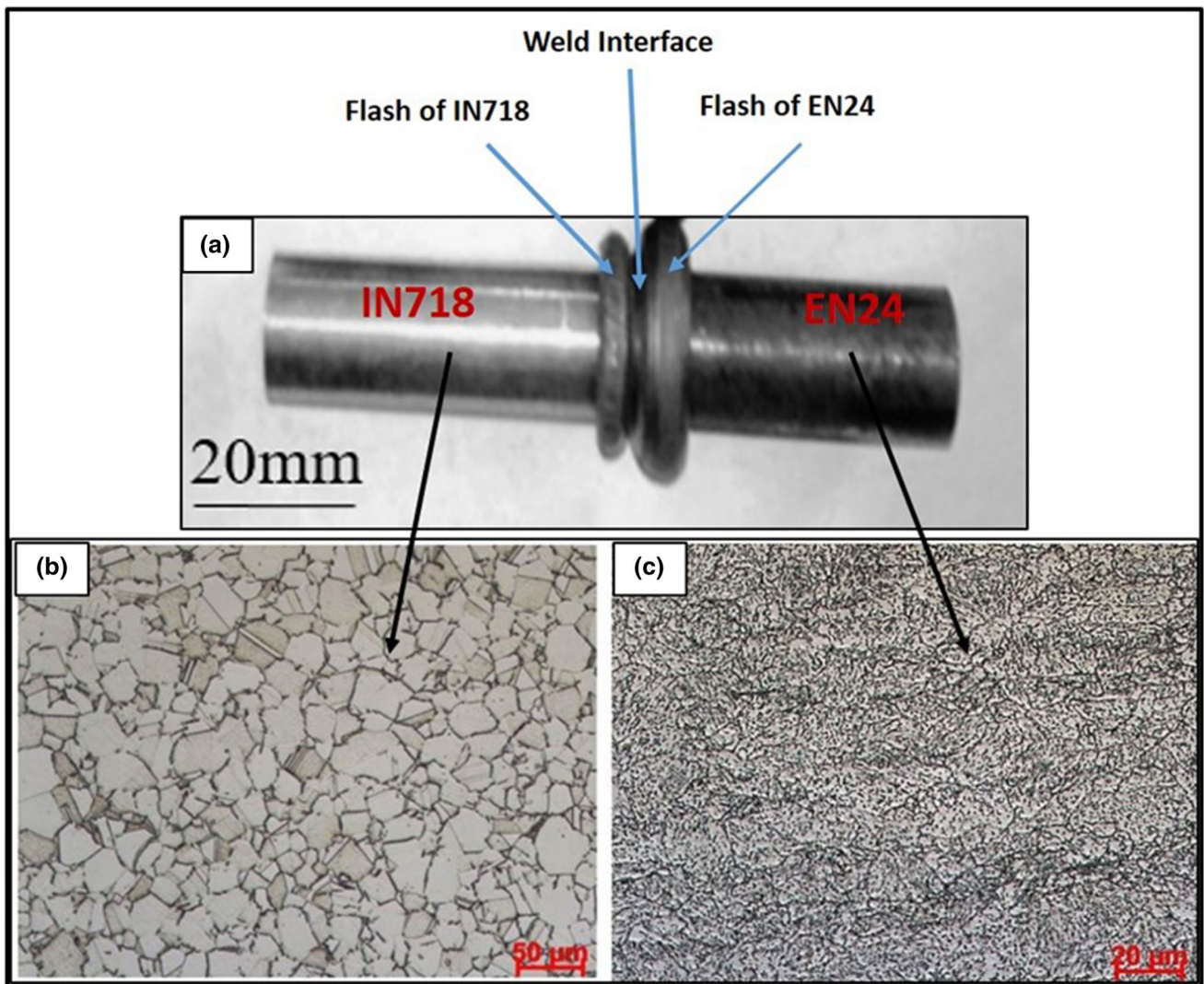


Fig. 2 (a) Image of friction-welded joints of IN718 and EN24; microstructures of base metals: (b) IN718 and (c) EN24

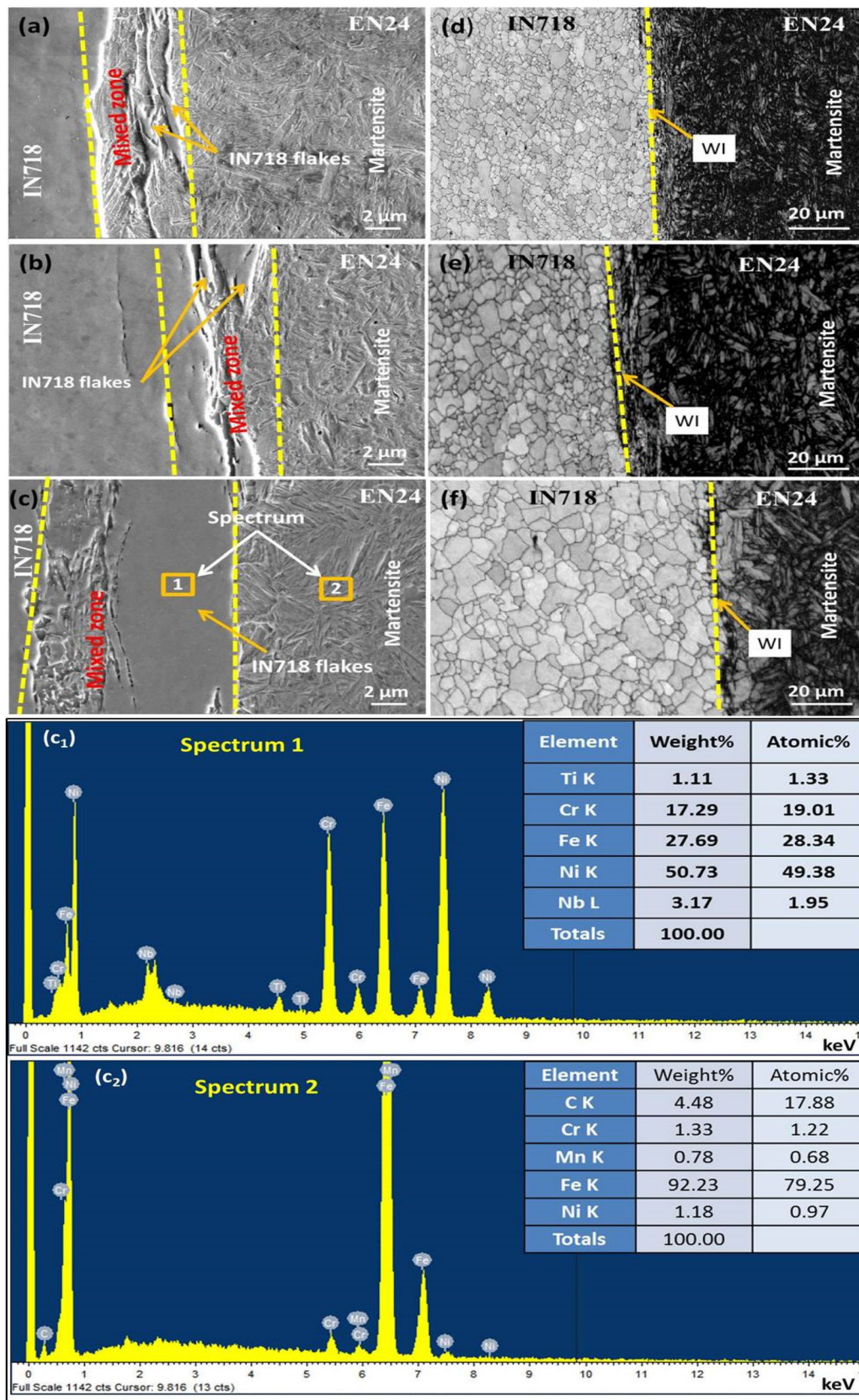


Fig. 3 SEM micrographs (a-c) and EBSD image quality maps (d-f) of FW joints of different friction times (a) 2 s, (b) 6 s, (c) 10 s, respectively; SEM-EDS spectrum (c₁) at location 1 and (c₂) at location 2

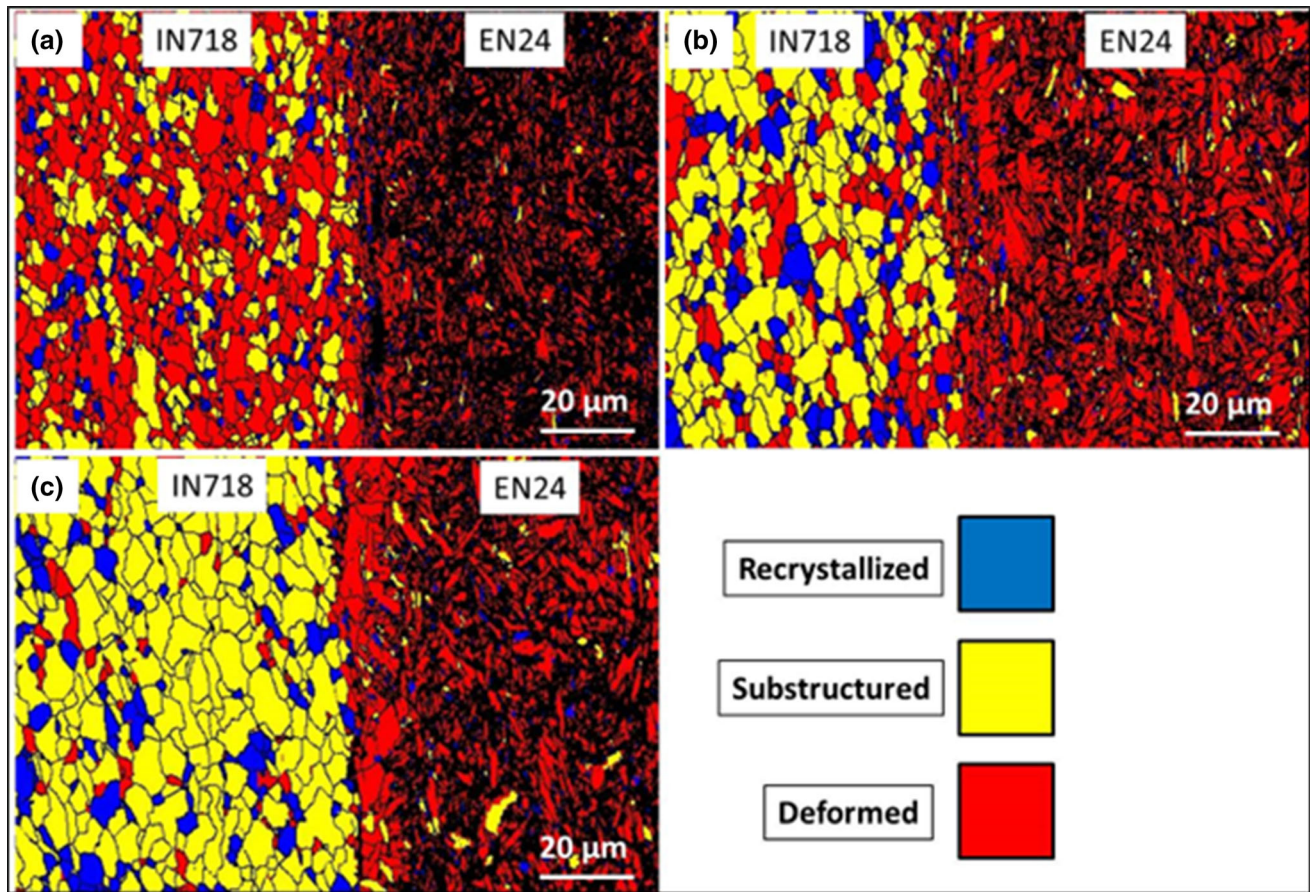


Fig. 4 Distribution of recrystallized, substructured and deformed grains in the WI/TMAZ regions of friction welded samples of different friction time (a) 2 s, (b) 6 s and (c) 10 s

Table 2 The fraction of recrystallized, substructured and deformed grains of FW samples

FW (different times), s	Location	Recrystallized grains, %	Substructured grains, %	Deformed grains, %
2	IN718—WI/TMAZ	10.8	27.6	61.5
6	IN718—WI/TMAZ	14.5	53.4	32.1
10	IN718—WI/TMAZ	17.3	75.5	7.2
2	EN24—WI/TMAZ	8.9	2.3	88.7
6	EN24—WI/TMAZ	6.7	4.0	89.2
10	EN24—WI/TMAZ	6.1	6.7	87.0

to austenite region due to heat generated from friction and deformation (Ref 17, 18). It may be noted that self-quenching occurs from the bulk material resulting a solid-state phase transformation of austenite to martensite. Furthermore, the mechanically mixed zone is clearly visible for the welded joints. This zone consists of intermixture of both the base materials. In order to get qualitative information of joint, energy-dispersive x-ray spectroscopy (EDS) studies were carried out (Fig. 3c₁ and c₂). It may be noted that locations 1 and 2 (shown in Fig. 3c) belong to IN718 and Fe-rich region, respectively.

EBSD image quality maps of WI/TMAZ are shown in Fig. 3(d-f). These zones are strongly affected by the heat and plastic deformation that causes dynamic recrystallization. The distribution of recrystallized, substructured and deformed

grains of samples welded with different friction times 2 s, 6 s and 10 s is presented in Fig. 4, and the percentage of these grains are given in Table 2. The percentages of substructured grains of IN718 side are higher as compared with EN24 side, indicating that major recovery occurred on IN718 side. The highest percentage of substructured grains (75.5%) was observed in 10 s samples. Moreover, the deformed grains on WI/TMAZ of EN24 side are dominating which may be due to formation of martensite. From the above investigation, it can be seen that the grains in WI/TMAZ are strongly affected by the thermo-mechanical effect.

3.2 X-ray Diffraction Analysis

The x-ray diffractograms obtained from base materials and weld interface of different samples (friction time: 2 s, 6 s and

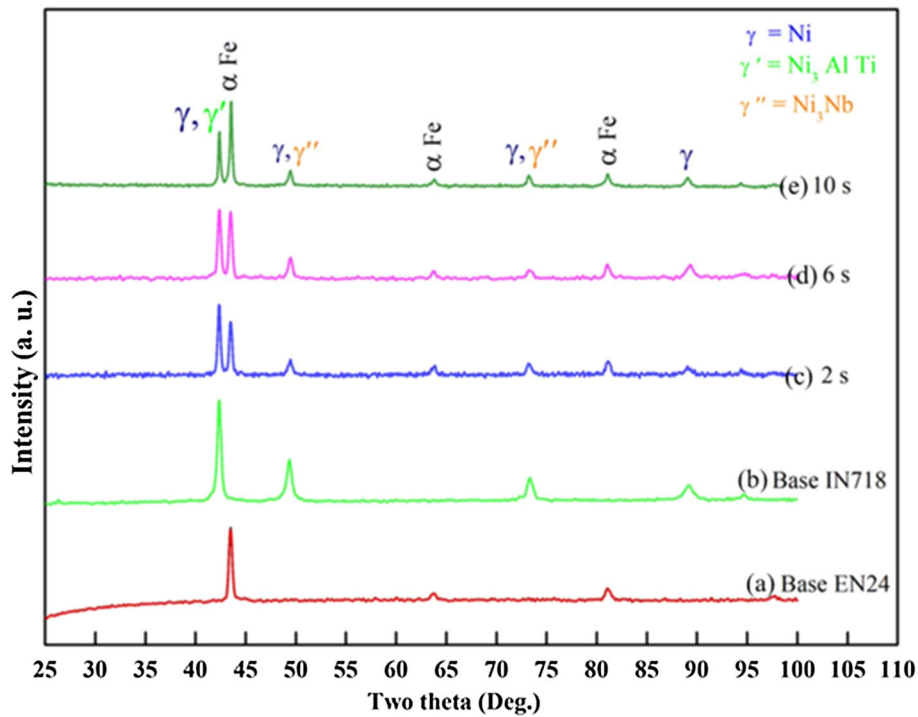


Fig. 5 X-ray diffractograms of base metal (a) EN24, (b) IN718 and welded samples of different friction time (c) 2 s, (d) 6 s and (e) 10 s

Table 3 Burn-off length of FW samples welded with different friction time

Friction time, s	Initial length (Li), mm	Final length (Lf), mm	Burn-off length (Lo) = (Li-Lf), mm	Burn-off length (Lo) = (Li-Lf)/Lf * 100, %
2	130.2	125.0	5.2	4.2
4	130.3	124.0	6.7	5.1
6	129.4	120.5	9.0	7.4
8	130.8	119.3	12.3	9.6
10	130.3	115.4	15.0	12.9

10 s) are presented in Fig. 5. The base metal of EN 24 sample contains intensity peaks of (110), (200) and (211) planes corresponding to α -ferrite. However, IN718 base metal has intensity peaks of (111), (200) and (220) planes corresponding to γ phase and intensity peaks (111), (121) planes corresponding to strengthening precipitates γ' and γ'' , respectively. It can be seen that as the friction time increases, intensity peaks of γ' and γ'' decrease, indicating dissolution of strengthening precipitates. These dissolve precipitates (γ' and γ'') affect mechanical property as discussed in Section 4.1.

3.3 Effect of Friction Time on Burn-Off Length

The images of FW samples welded at different friction time are illustrated in Fig. 1(b). It can be seen that the flash geometries are asymmetrical and flash width increases with friction time. Asymmetrical flash width is associated with difference in thermal conductivity and strengths of IN718 and EN24. During FW, the temperature of EN24 side is experiencing higher as compared to IN718 due to lower thermal conductivity of EN24 (Ref 8). As a result, EN24 side becomes more softer and forms more amount of flash. However if the friction time is excessively short, then the heating effect

becomes ineffective which causes to form unbounded regions. It may also be noted that higher friction time leads to higher material lost in terms of flash. Peng Li et al. studied the effect of friction time on the mechanical and metallurgical properties of continuous drive friction-welded (Ti6Al4V/SUS321) joints. They observed that excess heating time in the FW increases material consumption and grain coarsening (Ref 14). It can be seen that at the starting of the welding process (2 s), lower burn-off length was observed. However as the welding time increases, burn-off length for the friction time (2-10 s) increases from 4.2 to 12.9%. The heat accumulated through friction is adequate to soften the base metals and therefore increases flash formation.

The burn-off length of welded samples is shown in Table 3, which follow the following equation,

$$L = 1.26t + 2.08 \quad (\text{Eq 1})$$

where L = burn-off length (mm), and t = friction time (s).

Equation 1 depicts the change of burn-off length with respect to friction time. The burn-off length and friction time are linearly dependent (correlation coefficient value of 0.992) as shown in Fig. 6.

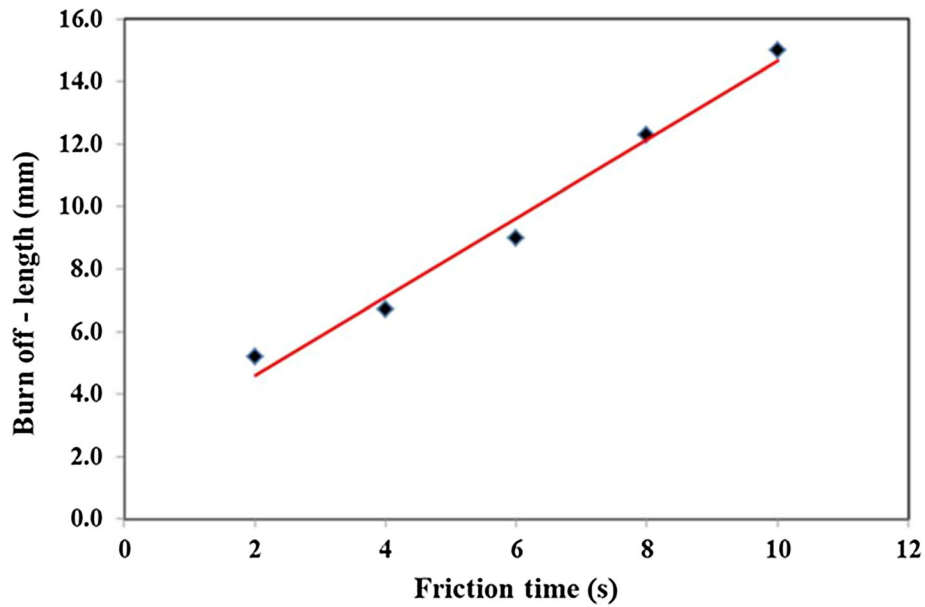


Fig. 6 Variation of burn-off length with friction

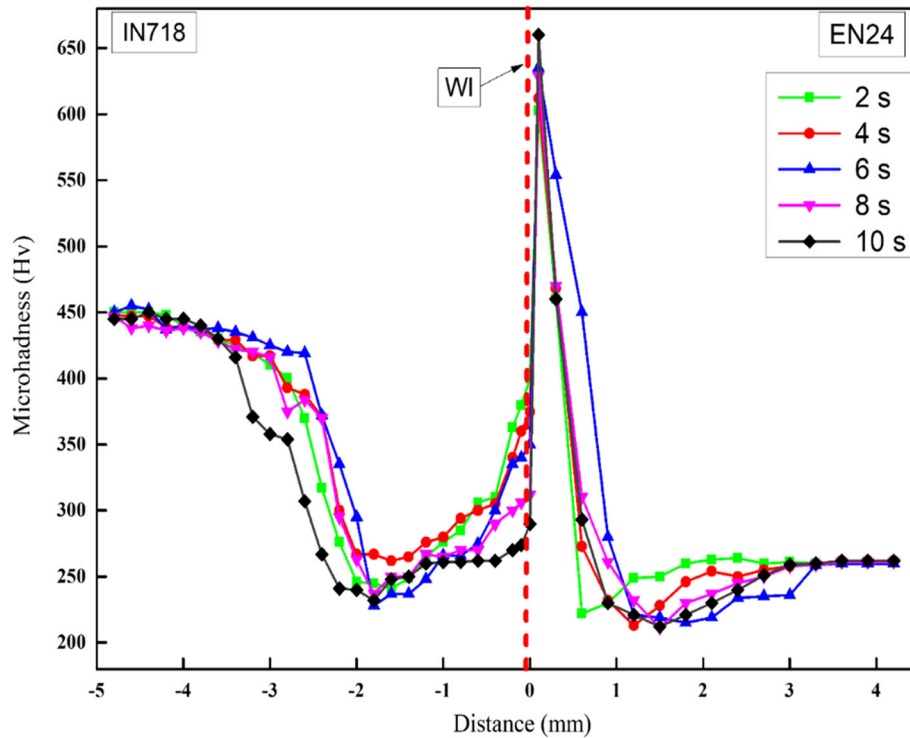


Fig. 7 Microhardness distribution across the WI of different welded samples

4. Mechanical Properties

4.1 Microhardness Distribution

The microhardness measurements across WI are shown in Fig. 7. All samples show almost similar hardness profile. However, peak hardness was observed in WI/TMAZ of the EN24 side. Compared with base material of EN24, WI/TMAZ showed hardness improvement of about 149%. This significant

rise in hardness is attributed to formation of martensite as shown in Fig. 8(a) and (b).

It was also observed that hardness in HAZ area was lower than that of IN718 base metal. Further, longer the friction time reduces the hardness of WI/TMAZ. The base metal consists of strengthening precipitates (γ' and γ'') as well as a delta (δ) phase as shown in Fig. 8(c) and (d). In the literature, researchers have done detailed investigation by using SEM/transmission electron microscope (TEM) about these strengthening precipitates in IN718 superalloy. The spherical-

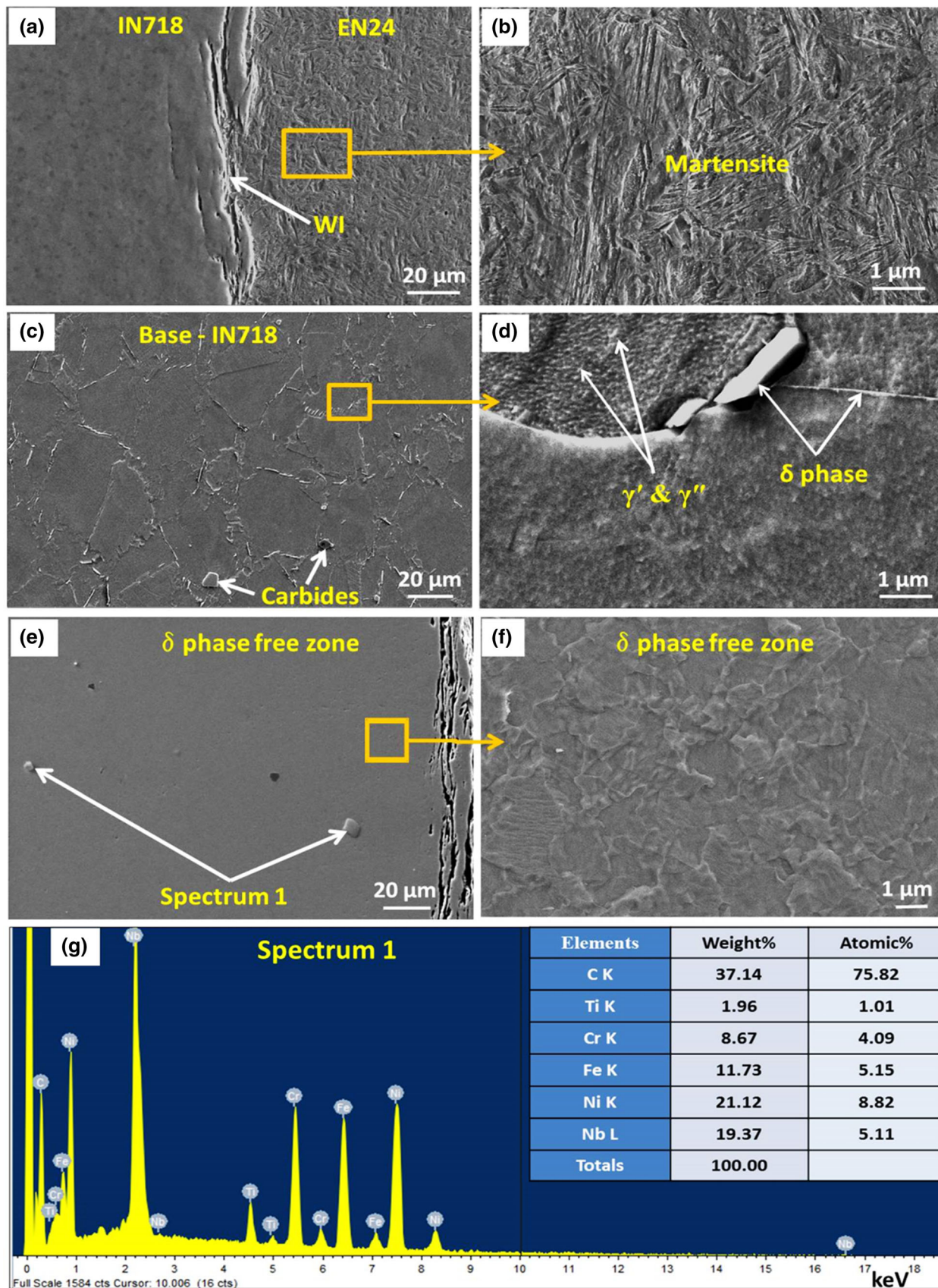
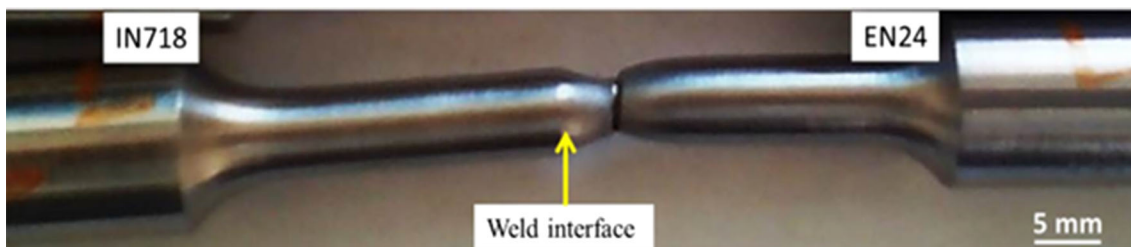


Fig. 8 SEM micrographs of friction welded (6 s) samples:- (a) WI/TMAZ, (b) WI/TMAZ of EN24 side, (c) IN718 base, (d) magnified image of IN718 base, (e) WI/TMAZ of IN718, (f) magnified image of WI/TMAZ of IN718 side and (g) EDS spectrum—at WI/TMAZ of IN718 side

Table 4 Mechanical properties of base metals and weld samples

Samples	Friction time, s	Yield strength, MPa	Ultimate tensile strength, MPa	Elongation, %	Joint efficiency, %
1	2	662.0 ± 15.0	750.0 ± 17.0	15.3 ± 2.0	97.7
2	4	665.0 ± 10.0	761.0 ± 9.0	14.0 ± 1.5	99.0
3	6	681.0 ± 6.0	772.0 ± 10.0	14.8 ± 1.0	100
4	8	650.0 ± 20.0	754.0 ± 15.0	14.8 ± 2.0	98.3
5	10	648.0 ± 20.0	752.0 ± 18.0	13.8 ± 2.5	98.0
Base – IN718	...	1188.0 ± 8.0	1374.0 ± 9.0	24.0 ± 3.0	...
Base – EN24	...	675.0 ± 7.0	767.0 ± 15.0	22.0 ± 1.5	...

**Fig. 9** Tensile tested sample (welded IN718 and EN24) showing failure location

shaped γ' precipitate with face-centered cubic (FCC) crystal structure is the secondary strengthening phase ($\sim 4\text{-}6\%$) of this superalloy (Ref 3). But, the primary strengthening of this alloy is obtained by disk-shaped γ'' precipitates with body-centered tetragonal (BCT) crystal structure ($\sim 15\text{-}20\%$) (Ref 11). After exposure at high temperature ($> 650\text{ }^\circ\text{C}$), the metastable γ'' phase can be transferred to stable needle-shaped delta (δ) phase. The delta (δ) phase is generally precipitates at grain boundaries and has the same composition as that of γ'' (Ni_3Nb) (Ref 5, 8). These phases are shown in Fig. 8(d). The needle-shaped delta phase (δ) is clearly seen along the grain boundaries. However the γ' , γ'' precipitates are shown inside the grains.

Since base metal is not affected by heat and deformation, it shows as-received hardness of 440 Hv. The reduction in hardness of WI/TMAZ occurred due to the dissolution of strengthening precipitates (γ' and γ'') and delta (δ) phase as shown in Fig. 8(e) and (f). However, as confirmed by EDS, some undissolved carbides (Fig. 8e and g) were present at IN718 side -WI/TMAZ zone.

4.2 Tensile Properties

Tensile test was performed to evaluate the strengths of the welded joints. It can be seen from Table 4 that welded sample has comparable strength corresponding to that of EN24. However, due to the formation of martensite in the weld zone, ductility was reduced. It was observed that samples failed in EN24 side at the interface of base and HAZ region away from the WI as shown in Fig. 9. This indicates weld zone is stronger than the weakest base metal (EN24). The joint efficiency (η) of the welded joint can be defined as the ratio of the tensile strength of weld joint to the tensile strength of soft material (Ref 16). Joint efficiency $\sim 100\%$ can be achieved by this welding technique.

The fractographs of tensile tested base materials (IN718 and EN24) and the FW joints (2 s, 6 s and 10 s) are presented in Fig. 10. The fracture appearance of base IN718 contains dimples, and some fracture channels marked with red and

yellow arrows, respectively, shown in Fig. 10(a). On the other hand, the fractographs of base EN24 show relatively dense small-sized dimples surrounded with few coarse size dimples marked by red and blue arrows, respectively, shown in Fig. 10(b).

It may be noted that the morphology of all welded fractured samples is similar to that of the base EN24. The EDS spectrum of tensile tested sample (Fig. 10e) is shown in Fig. 10(f). The major elements by weight percent are Fe, Ni, Cr and Mn, which confirm that the welded samples failed in the base metal of EN24 side.

5. Conclusions

The present research work is based on the continuous drive friction welding of IN718 and EN24 joints. By analyzing metallurgical and mechanical properties, the following conclusions can be drawn:

- Friction-welded joints show uneven flash width. The burn-off length mainly occurred in EN24 side. The minimum and maximum burn-off length was observed to be 5.2 mm and 15.0 mm with friction time 2 s and 10 s, respectively. Burn-off length at different friction times follows a simple linear equation: $L = 1.26t + 2.08$.
- The EBSD results reveal that the weld joints are strongly affected by thermo-mechanical effect with mostly deformed grains ($\sim 88\%$) and were observed in WI / TMAZ of EN24 side, while substructured grains in highest percentage ($\sim 75.5\%$) were observed in WI / TMAZ of IN718.
- XRD studies reveal that as the friction time increases, the dissolution of strengthening precipitates γ' ($\text{Ni}_3(\text{Al}, \text{Ti})$) and γ'' (Ni_3Nb) and the formation of martensite phase increases.
- Peak hardness was observed in EN24 side WI/TMAZ

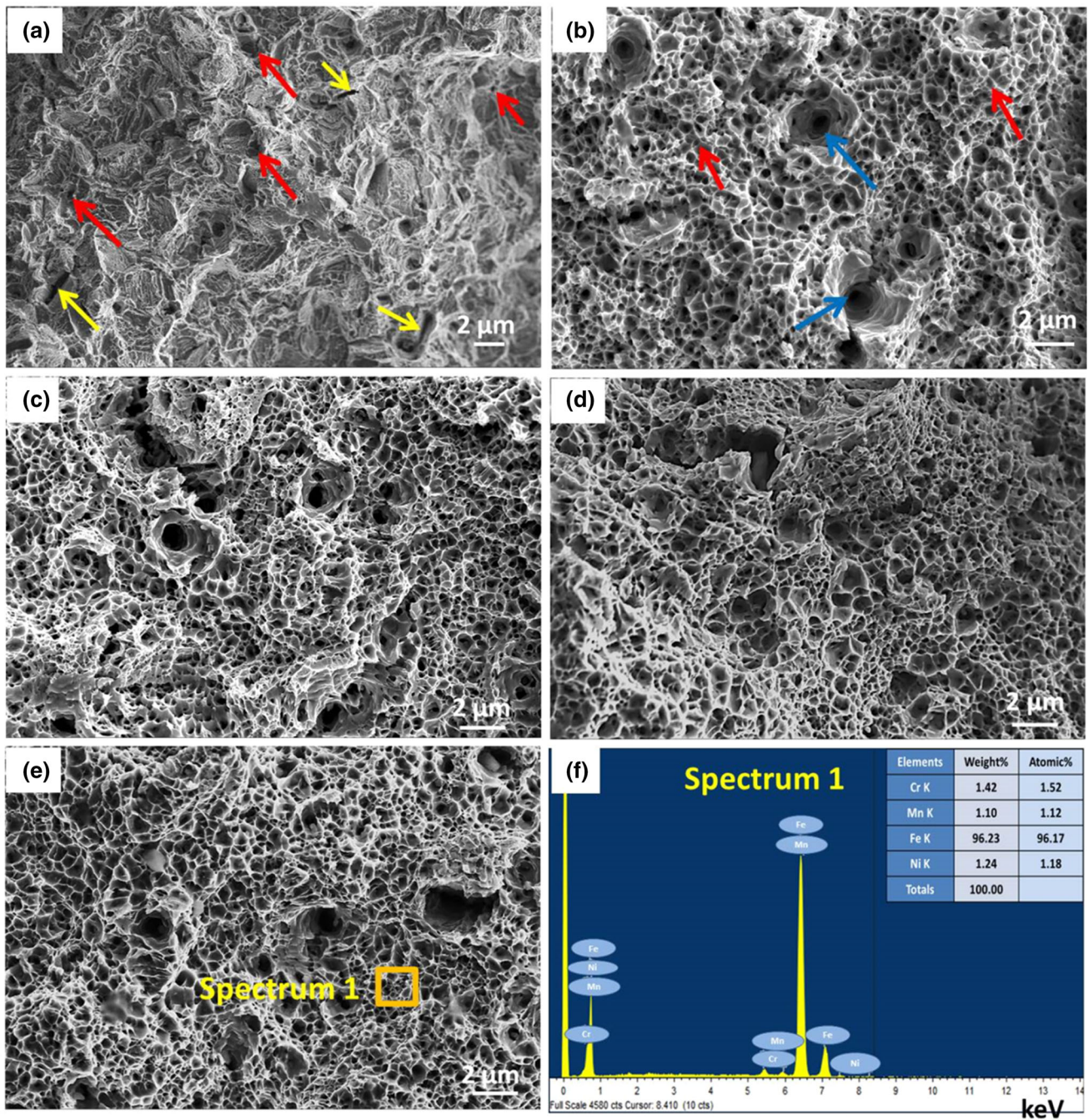


Fig. 10 Fractographs of different samples (a) base IN718, (b) base EN24 and welded samples of different friction times (c) 2 s, (d) 6 s, (e) 10 s and (f) EDS spectrum at fractured surface

areas because of martensite phase. The hardness of WI/TMAZ of IN718 was observed contrary as compared to that of EN24. The decreased hardness of WI/TMAZ of IN718 is attributed to dissolution of strengthening precipitates.

- The ultimate tensile strength of welded joint is found equivalent to that of EN24 base metal. The tensile sample failed in EN24 side at the interface of base and HAZ region.

Acknowledgments

The authors gratefully acknowledge to Kalyani Centre for Technology & Innovation (KCTI), Bharat Forge Ltd, Pune, and Department of Scientific and Industrial Research (DSIR), Govt. of India, for providing financial funding, laboratory and library facilities. The authors would like to express special thanks and gratitude to review committee of Bharat Forge Ltd, Pune, for granting the permission to publish this research work and also grateful to Mr. Vinayak Pawar and Mr. Santosh Dhage for their support in various aspects for this study. Also, the authors would like thank to Mr. Yatin Tambe, Director of Friction Welding

Technologies Pvt. Ltd., Pune, for providing friction welding facilities.

References

1. S.D. Meshram, T. Mohandas, and G. Madhusudhan Reddy, Friction Welding of Dissimilar Pure Metals, *J. Mater. Process. Technol.*, 2007, **184**, p 330–337
2. M. Anitha, C. Majumder, V. Saravanan, and S. Rajakumar, Microstructural Characterization and Mechanical Properties of Friction-Welded IN718 and SS410 Dissimilar Joint, *Metallogr. Microstruct. Anal.*, 2018, **7**, p 277–287
3. M.J. Donachie and S.J. Donachie, *Superalloys: A Technical Guide*, ASM International, Helsinki, 2002
4. J. Woolman and R.A. Mottram, *The Mechanical and Physical Properties of the British Standard EN Steels (BS 970–1955), EN 40 to EN 363*, Elsevier, Amsterdam, 2013
5. V. Ajay, N. Kishore Babu, M. Ashfaq, T. Mahesh Kumar, and K. Vamsi Krishna, A Review on Rotary and Linear Friction Welding of Inconel Alloys, *Trans. IIM*, 2021, **74**, p 1–16
6. J.C. Lippold, S.D. Kiser, and J.N. Du Pont, *Welding Metallurgy and Weldability of Nickel-Base Alloys*, Wiley, Hoboken, New Jersey, 2009
7. W. Li, A. Vairis, M. Preuss, and T. Ma, Linear and Rotary Friction Welding Review, *Int. Mater. Rev.*, 2016, **61**(2), p 71–100
8. V.T. Gaikwad, M.K. Mishra, V.D. Hiwarkar, and R.K.P. Singh, Microstructure and Mechanical Properties of Friction Welded Carbon Steel (EN24) and Nickel-based Superalloy (IN718), *Int. J. Miner. Metall. and Mater.*, 2021, **28**, p 111–119
9. H.C. Dey, M. Ashfaq, A.K. Bhaduri, and K. Prasad Rao, Joining of Titanium to 304L Stainless Steel by Friction Welding, *J. Mater. Process. Technol.*, 2009, **209**, p 5862–5870
10. J.S. Tiley, D.W. Mahaffey, T. Alam, T. Rojhirunsakool, O. Senkov, T. Parthasarthy, and R. Banerjee, Strengthening Mechanisms in an Inertia Friction Welded Nickel-Base Superalloy, *Mater. Sci. Eng. A*, 2016, **662**, p 26–35
11. R. Damodaram, S.G.S. Raman, and K.P. Rao, Microstructure and Mechanical Properties of Friction Welded Alloy 718, *Mater. Sci. Eng. A*, 2013, **560**, p 781–786
12. W. Hongjie, K. Ikeuchi, M. Aritoshi, M. Takahashi, and A. Ikeda, Joint Strength of Inconel 718 Alloy and its Improvement by Post-Weld Heat Treatment-Joint Performance and its Controlling Factors in Friction Welding of Inconel 718 Alloy, *Weld. Int.*, 2009, **23**, p 679–686
13. S.V. Lalam, G.M. Reddy, T. Mohandas, M. Kamaraj, and B.S. Murty, Continuous Drive Friction Welding of Inconel 718 and EN24 Dissimilar Metal Combination, *Mater. Sci. Technol.*, 2009, **25**, p 851–861
14. P. Li, J. Li, M. Salman, L. Liang, J. Xiong, and F. Zhang, Effect of Friction Time on Mechanical and Metallurgical Properties of Continuous Drive Friction Welded Ti6Al4V/SUS321 Joints, *Mater. Des.*, 2014, **56**, p 649–656
15. D. Meshram Suresh and G. Madhusudhan Reddy, Friction Welding of AA6061 to AISI 4340 Using Silver Interlayer, *Def. Technol.*, 2015, **11**, p 292–298
16. O. Tomo, K. Miyoshi, T. Matsumura, T. Imai, and K. Saida, Improvement of Joint Strength in Dissimilar Friction Welding of Ti-6Al-4V Alloy to Type -718 Nickel-Based Alloy Using the Au-Ni Interlayer, *Sci. Technol. Weld. Join.*, 2019, **24**, p 327–333
17. J.T. Yeom, J.H. Park, J.W. Lee, and N.K. Park, Characterization of Friction Welding for IN713LC and AISI 4140 Steel, *Mater. Sci. Forum*, 2004, **449**, p 53–56
18. V.T. Gaikwad, V.D. Hiwarkar, V.P. Pawar, and R.K.P. Singh, Microstructure Characterization and Evaluation of Mechanical Properties for Friction Welded EN-24 Alloy Steel, Contributed Papers From Materials Science and Technology Oct 14–18, (Columbus, Ohio, USA, 2018), p 822
19. C. Billel, D. Miroud, R. Badji, P. Hvizdos, M. Fides, T. Csanadi, B. Belkessa, and M. Tata, Microstructure and Mechanical Behavior of Dissimilar AISI 304L/WC-Co Cermet Rotary Friction Welds, *Mater. Sci. Eng. A*, 2019, **758**, p 36–46
20. L. Huihong, Yo. Aoki, Y. Aoki, K. Ushioda, and H. Fujii, Principle for Obtaining High Joint Quality in Dissimilar Friction Welding of Ti-6Al-4V Alloy and SUS316L Stainless Steel, *J. Mater. Sci. Technol.*, 2020, **46**, p 211–224
21. Z. Changqing, S. Wang, D. Luo, W. Shi, X. Liu, G. Cui, B. Chen, Z. Xin, and Z. Rui, Study of the Mechanical Properties and Microstructures of Conical Joints for Aluminum/Steel Continuous Drive Friction Welding, *J. Manuf. Process.*, 2021, **67**, p 241–252

Publisher's Note Springer Nature remains neutral with regard to jurisdictional claims in published maps and institutional affiliations.

Springer Nature or its licensor holds exclusive rights to this article under a publishing agreement with the author(s) or other rightsholder(s); author self-archiving of the accepted manuscript version of this article is solely governed by the terms of such publishing agreement and applicable law.